UNIVERSITY OF BIRMINGHAM
University of Birmingham Research at Birmingham

Volumetric generation of optical vortices with metasurfaces

Huang, Lingling; Song, Xu; Reineke, Bernhard; Li, Tianyou; Li, Xiaowei; Liu, Juan; Zhang, Shuang; Wang, Yongtian; Zentgraf, Thomas

DOI:
10.1021/acsphotonics.6b00808

License:
None: All rights reserved

Document Version
Peer reviewed version

Citation for published version (Harvard):
Huang, L, Song, X, Reineke, B, Li, T, Li, X, Liu, J, Zhang, S, Wang, Y & Zentgraf, T 2017, 'Volumetric generation of optical vortices with metasurfaces', *ACS Photonics*, vol. 4, no. 2, pp. 338-346. https://doi.org/10.1021/acsphotonics.6b00808

Link to publication on Research at Birmingham portal

General rights
Unless a licence is specified above, all rights (including copyright and moral rights) in this document are retained by the authors and/or the copyright holders. The express permission of the copyright holder must be obtained for any use of this material other than for purposes permitted by law.

•Users may freely distribute the URL that is used to identify this publication.
•Users may download and/or print one copy of the publication from the University of Birmingham research portal for the purpose of private study or non-commercial research.
•User may use extracts from the document in line with the concept of 'fair dealing' under the Copyright, Designs and Patents Act 1988 (?)
•Users may not further distribute the material nor use it for the purposes of commercial gain.

Where a licence is displayed above, please note the terms and conditions of the licence govern your use of this document.

When citing, please reference the published version.

Take down policy
While the University of Birmingham exercises care and attention in making items available there are rare occasions when an item has been uploaded in error or has been deemed to be commercially or otherwise sensitive.

If you believe that this is the case for this document, please contact UBIRA@lists.bham.ac.uk providing details and we will remove access to the work immediately and investigate.

Download date: 02. May. 2024

DOI:
Article type: Communication

Title: Three-dimensional vortex array generation with dielectric geometric metasurfaces

Lingling Huang[1], Xu Song[1], Bernhard Reineke[2], Tianyou Li[1], Xiaowei Li[3], Juan Liu[1], Shuang Zhang[4], Yongtian Wang[1]*, Thomas Zentgraf[2]**

Dr. Lingling Huang, Xu Song, Tianyou Li, Prof. Juan Liu, Prof. Yongtian Wang
1 School of Optoelectronics, Beijing Institute of Technology, Beijing 100081, China
E-mail: huanglingling@bit.edu.cn; wyt@bit.edu.cn
Bernhard Reineke, Prof. Thomas Zentgraf
2 Department of Physics, University of Paderborn, Warburger Straße 100, D-33098 Paderborn, Germany
E-mail: thomas.zentgraf@upb.de
Dr. Xiaowei Li
3 Laser Micro/Nano-Fabrication Laboratory, School of Mechanical Engineering, Beijing Institute of Technology, Beijing 100081, China
Prof. Shuang Zhang
4 School of Physics & Astronomy, University of Birmingham, Birmingham, B15 2TT, UK

Keywords: dielectric metasurfaces, vortex beam, parallel processing, optical communications

Abstract: Recent advances in metasurfaces, i.e., two dimensional arrays of engineered nanoscale inclusions that are assembled onto a surface, have revolutionized the way to control electromagnetic waves with ultrathin, compact components. The generation of optical vortex beams, which carry orbital angular momentum, has emerged as a vital approach to applications ranging from high-capacity optical communication to parallel laser fabrication. However, the typically bulky elements used for the generation of optical vortices impose a fundamental limit toward on-chip integration with subwavelength footprints. Here, we investigate and experimentally demonstrate a three-dimensional vortex array generation based on the light-matter-interaction with a high-efficiency dielectric metasurface. By employing the concepts of Dammann vortex gratings and spiral Dammann zone plates, 3D optical vortex arrays with micrometer spatial separation are achieved from visible to near-infrared

wavelengths. Importantly, we show that the topological charge distribution can be spatially variant and be fully controlled by the design.

Main Text:

Flat optics have attracted great interest for being a promising alternative to control light waves by implementing ultrathin planar elements, namely metasurfaces, with spatially varying phase response instead of relying on phase accumulation along optical paths [1-3]. The main advantage of such tailored metasurfaces is that large phase shifts can be realized by nanostructures with thicknesses much less than the wavelength of light, and thus metasurface can be easily integrated into multifunctional on-chip optoelectronic systems [4-6]. Particularly, one type of such metasurfaces, referred to as geometric metasurfaces (GMs) that are based on a Pancharatnam-Berry phase change principle, provide fascinating dispersion-less and helicity-dependent phase properties [7-9]. The desired phase profile of the wave is directly encoded in the azimuthal orientation of the locally imprinted meta-atom [9-10]. The recent advances in flat optics with metasurfaces have shown the ability to overcome the limitations of conventional optics with a wide range of applications in wave front engineering [11-17], information processing [18], and spin controlled photonics [19-21]. In principle, the phase profiles of nearly any optical components including lenses [11-13], wave plates [14], holograms [15-16], as well as elements capable of bending light in unconventional ways [17] could be designed on the basis of plasmonic or dielectric metasurfaces [22-23].

An important application for metasurfaces is the control and modification of optical beam profiles, and in particular the generation of orbital angular momentum (OAM) for light, which is important in terms of both fundmental physics and practical applications. The optical vortex beam that possesses a helical phase front and a doughnut-shaped intensity in the focus spot [24-25] has received increasing attention for its various applications, ranging from optical manipulation of microscopic particles and biological cells [26] to free-space optical

communication system [27]. Such a beam is characterized by an azimuthal phase dependence $exp(il\varphi)$, i.e., the OAM in the propagation direction has the discrete value of l per photon, where l is the topological charge of the beam [24]. Various techniques have been reported for the generation of optical vortices, such as spiral phase plates, spatial light modulators, cylindrical mode converter and computer-generated holograms [25]. However, bulky macro-scale interference-based generation methods through hologram-coding or phase-shifting have imposed a fundamental physical limit for realizing the vortex beam at a chip-scale footprint. In recent studies, metasurfaces with phase-modification capability were used for optical vortex generation, which showed potential for significant size reduction of the optical elements [4,9,28-30]. However, those vortex plates were so far restricted to create only limited number of vortices with specific topological charges [4,9,28-30], whereas spatial multiplexing would be required to attain additional topological charges [28].

As the various values of OAM of optical vortex beams result in different orthogonal eigenmodes they have gained great attention for optical multiplexing to facilitate a dramatic increase in transmission capacity by exploring the spatial freedom of light waves [27,31-33]. Especially, it has been shown that the use of vortex beams with an OAM basis can increase the tolerance of quantum key distribution systems to eavesdropping [34]. A number of schemes have been proposed for the parallel processing of vortex beams, including free space multiplexing and demultiplexing of OAM eigenstates [35], chip-scale generation and transmission of OAM-carrying beams on silicon-integrated circuits through whispering gallery mode resonators [31-32] and waveguide-based interconnected resonant microring fibers [33]. However, these approaches are resonant and therefore highly dispersive in nature, leading to a narrow bandwidth down to several nanometers. In addition, these techniques are not suitable for achieving a truly three-dimensional (3D) parallel processing of vortex beams with a more compact footprint.

In this letter, we propose and experimentally demonstrate the generation of a three-dimensional vortex array with independently controllable topological charges that is based on a single ultrathin dielectric metasurface. We employ the concepts of Dammann vortex grating [36-37] and spiral Dammann zone plate [38] together with a lens factor to generate the metasurface phase profile with subwavelength pixel size. Figure 1 illustrates the generation and reconstruction procedure of such a 3D vortex array. The metasurface consists of Silicon nanofins patterned on top of a glass substrate. Each nanofin acts as a pixel of the entire diffractive metasurface element that generates the required continuous local phase discontinuity for circularly polarized (CP) light at normal incidence. The generated 3D vortex array with spatially variant topological charges is designed to appear within the Fresnel range of the metasurface. Specifically, the topological charge in each node of the generated 3D lattice can be determined by a simple formula $mL_x+nL_y+qL_z$, where m, n and q represent the diffraction orders in x, y, and z directions, and L_x, L_y and L_z are the intrinsic base topological charges in transverse and longitudinal directions, respectively (Supplementary Materials). The design technique allows for a well-defined, quantized, and fully controllable spatially variant topological charge distribution. Importantly, such metasurface based vortex generators can achieve truely 3D vortex arrays over a large volume with high uniformity. Furthermore, the geometric nature of the phase profile (based on a Pancharatnam-Berry-Phase) enables the reconstruction of the vortices over a broad spectral bandwidth in the near-infrared and visible wavelength range. Importantly, the metasurface can be designed to possess the remarkable capability of vortex beam detection. The flexibility of our approach enables on-chip parallel processing to 3D micro- and nano-fabrication [39], and offers the possibility of ultrahigh-capacity and miniaturized nanophotonic devices for harnessing angular momentum multiplexing and mode sorting [40-41].

The design principle of the vortex plate is schematically shown in Figure 2. The phase distribution is obtained from the combination of an optimized Dammann Vortex Grating

(DVG), a Spiral Dammann Zone Plate (SDZP), and a lens factor, as shown in Figure 2(a) (Supplementary Materials). The DVG is particularly designed to create a two-dimensional vortex array in the *x*-*y* plane with uniform energy distribution among the designated diffraction orders. This is accomplished by integrating the blazing grating with a spiral phase pattern with intrinsic base topological charge of L_x and L_y in orthogonal directions, whereas each period is divided into equal segments for multi-level phase optimization with a simulated annealing algorithm to achieve better uniformity. Each diffraction order (*m*, *n*) in the transverse focal plane is characterized by an equal-energy optical vortex of topological charge mL_x+nL_y. The SDZP can achieve a sequence of coaxial vortices in the focal volume. Indeed, a SDZP is essentially a Dammann zone plate (DZP) into which a spiral phase structure with intrinsic base topological charge of L_z is nested. In analogy to the Dammann grating concept, by modulating the phase transition points in one period in radial direction of the SDZP, the light energy can be redistributed uniformly into several longitudinal coaxial vortices at the desired orders. In addition, a lens factor is also nested into the final phase mask to simplify the generation scheme of the vortex array, because traditionally one has to insert a lens in front of the SDZP. Thus a sequence of coaxial focused vortices carrying a topological charge of qL_z for q^{th} order can be generated longitudinally in the proximity of geometric focus, by combining the SDZP together with the lens factor. Note here the vortex located at the geometrical focal position of the lens is defined as zeroth order, whereas the vortices extending along the positive *z* direction are defined as positive orders and vice versa. Therefore, through overlapping these three phase profile of the DVG, the SDZP and the lens factor together, the final phase plate can be formed, which has the capacity to generate 3D vortex array with topological charge distribution obeying the rule of $mL_x+nL_y+qL_z$. Numerical simulations show the transverse and longitudinal coaxial vortices intensity distributions in both the focal plane (in *x*-*y* plane) and the meridian plane (in *y*-*z* propagation plane) for each single DVG (Figure 2b) and SDZP (Figure 2c), respectively. The effect of the

lens factor, which converges the scattered light from the SDZP into separate longitudinal coaxial positions in the neighbourhood of focus volume, is schematically illustrated by Figure 2d.

With such a design an M×N×Q 3D vortex array can be achieved by combining an M×N DVG and a 1×Q SDZP together with a lens factor, where M, N, and Q are numbers of total diffraction orders along three orthogonal orientations, respectively. To verify the concept of our design methodology, a 5×5 DVG with intrinsic base topological charge $L_x = L_y = 2$, a 1×5 SDZP with $L_z = 2$ and a lens factor with focal length $f = 800$ μm are chosen for experimental demonstration. The detailed design principle can be found in the Supplementary Material.

The vortex plate is realized by utilizing a dielectric geometric metasurface to encode the generated phase profile following the above design. The metasurface is composed by designed pattern of silicon nanofins on top of a glass substrate (Figure 3). Each single Si nanofin can be considered as a dielectric resonator, and its orientation dependent interaction with CP light generates the desired geometric phase discontinuity of $\Phi = 2\sigma\theta$ in the cross-polarized scattered field, where $\sigma = \pm 1$ corresponds to the helicity of right- (RCP) and left circularly polarized (LCP) incident light, and the azimuthal angle θ of the nanofin with respect to the laboratory frame [9]. It is well known that a half wave plate can fully convert a circularly polarized beam into the opposite handedness as the result of a phase delay of π between the fast and slow axes. Hence, to achieve high conversion efficiency between the two circular polarization states, we carry out a 2D parameter optimization using a rigorous coupled wave analysis method to optimize the size parameters of the nanofins. The lattice constant of the nanofin array was fixed to be 600 nm, and the length L to be 400 nm. The parameters for width and height of the Si nanofins are swept to find the optimum parameters for half-wave plate functionality at the operation wavelength of $\lambda = 780$ nm. For the refractive index of amorphous silicon (α-Si) at 780 nm a value of $n = 3.9231 + 0.1306i$ was used. The simulated conversion efficiency and phase difference δ between the fast and slow axes are

shown in Figure 3(b). Note that the conversion efficiency is defined as the ratio of the cross polarization efficiency to the total transmission efficiency composed of both co-polarization and cross polarization. The optimized values for the height h and width w of the Si nanofins are chosen as 450 nm and 140 nm, respectively, resulting in a high conversion efficiency of 57.2% and a phase delay of π at 780 nm.

For the experimental proof of the concept we fabricate the dielectric metasurface sample by standard electron beam lithography and reactive ion etching of Silicon (for details see Supplementary Material). The vortex plate contains 666×666 pixels, with a lattice constant of 600 nm. The fabricated Si nanofins have a size of 410×175×466 nm^3 (L×w×h), which are close to our designed values (Figure 3c).

For the characterization of the metasurface we first simulate the intensity distribution of vortex array in x-y plane at different focal planes along the z direction (Figure 4). The numerical calculations are performed by using a Fresnel diffraction method. From the intensity plots one can clearly observe that the characteristic beam profile for each vortex exhibits an annular intensity distribution in the cross section, and a characteristic dark spot with zero intensity in the center. Furthermore, an entire set of 5 focal planes along the z direction is achieved, whereas the 5×5 in-plane vortices on each plane are spatially variant. For further discussion we take the zeroth-order focal plane at z=815μm for λ=780 nm as an example. According to the rule of $mL_x+nL_y+qL_z$, we can easily determine that the distributions of topological charges should be symmetric about the diagonal line of such a 5×5 array with q=0. As an illustration, the topological charges in the first row can be calculated as [−8, −6, −4, −2, 0] by setting m=[−2, −1, 0, 1, 2], n=−2, q=0 . Each focused vortex beam shows quite distinct doughnut-shaped intensity distribution with a different radius. Similarly, the topological charge distribution at other focus planes can be calculated with the same method.

Experimentally we use a setup as shown in Figure 5(a). A linear polarizer (P) and a quarter wave plate (QWP) are positioned in front of and after the sample to prepare and select the desired circular polarization state for the illumination and transmission. Due to the sub millimetre size of the reconstructed vortex array, a 20× (NA=0.45) magnifying microscope objective is positioned right after the sample to collect the transmitted light and image it onto a CCD camera. The depth and spatial distribution of the 3D vortex lattice can be analysed by adjusting the 3D precision translation stage where the sample is mounted on. Thus, different focal planes can be imaged separately on the camera to obtain a series of 2D images, allowing the verification of the 3D vortex array located at the corresponding node of the 3D lattice.

Although the metasurface is designed for a wavelength of λ=780 nm (for which the metasurface functions as a half wave plate to efficiently enhance the conversion efficiency), it can also work at other wavelengths due to the dispersion-less phase property based on the Pancharatnam-Berry phase principle. We demonstrate this broadband effect by measuring the corresponding beam profiles for wavelengths of λ=633 nm and λ=785 nm at the q=0, 1, 2 planes (Figure 5(b)). We observe that the vortices with topological charge equal to zero shift their positions from the center diagonal line to the secondary diagonal and third diagonal, respectively. The experimental results show good agreement with the numerical predictions in Figure 4. More detailed measurement results can be found in the Supplementary Material.

Other performance parameters are characterized as well, including the transverse and axial focus spacing, uniformity, and efficiency. The transverse spacing in both x and y directions are equal to 100 μm as designed. On the other hand, the z positions for the coaxial planes for λ=785 nm are shifted from 598 μm, 689 μm, 815 μm, 997 μm, to 1281 μm, respectively. While for λ=633 nm the coaxial planes are shifted from 736 μm, 899 μm, 1003 μm, 1226 μm, to 1579 μm, respectively. The distances between the coaxial planes and the metasurface is approximately inverse-proportional to the wavelength, which can be explained from Fermat's principle. This simple relationship explains very well the experimental

observations as well as the actual z positions can be determined from the numerical calculations with the Fresnel diffraction theory. By applying the Dammann optimization scheme, the energy distribution for each vortex beam is quite uniform. By collecting the entire transmitted CP light with opposite handedness by a lens, we determined the overall energy efficiency. In particular, the transmission efficiency at λ=785 nm reach up to 59.1%, while the efficiency at λ=633 nm drops to 15.6%.

The metasurface can also be used for measuring the topological charge of a vortex beam (Figure 6). Light from the He-Ne laser with λ=633 nm is collimated and expanded through an objective and pinhole. By using a spatial light modulator (SLM), which is uploaded with a fork shaped phase profile (see inset of Figure 6) to generate the vortex beam of desired topological charge. When a b-charged vortex beam is selected as the incident beam, the topological charges of the 5 × 5 vortex arrays on those five coaxial planes can be determined by $mL_x+nL_y+qL_z+b$ (Figure 7). When the topological charge of the vortex array at a certain order is zero, the vortex will be annihilated, and the dark core disappears. Instead, in the far field, a central bright spot appears which can serve as the criteria for detection of the topological charge. For the experiment we utilized a vortex beam with topological charge of l=−4 to detect the corresponding vortices in the five coaxial planes. Thus, the corresponding vortex with l=4 would be quenched to be a bright focal point, as indicated by the green dashed lines in Figure 7. All the other vortices would acquire extra OAM of b . The experimental results confirm our theoretical expectations. The detailed results for incident vortex beam carrying different topological charges of l=0, −2, −4, and −6 can be found in the Supplementary Material.

Our presented generation mechanism of 3D vortex arrays is an efficient and simple method for generating spatially variant vortex beams. The experimental results show that the overall 5 × 5 × 5 vortex arrays are tuneable by simply changing the OAM of the incident beam. Such flexibility in operation implies that the vortex array on one certain cross-sectional

plane can be freely manipulated and fully controllable. Besides the 3D vortex array generation, the metasurface possesses the remarkable capability of topological charge detection in multiplexed vortex beams. It should be noted that the energy distribution of each vortex located in the corresponding node of the 3D lattice can be adjusted to be proportional rather than equally through multilevel continuous phase optimization in each segment of the metasurface plate. Therefore, it can provide greater freedom in applications such as 3D parallel laser fabrication.

In summary, we propose and experimentally demonstrate 3D vortex arrays with spatially variant topological charges. The concept was realized by an ultrathin dielectric geometric metasurface with chip-scale footprint as small as 400 μm^2. The dielectric metasurface with Si nanofins can work effectively as a half wave plate at the operation wavelength of 780 nm which leads to a high efficiency for the Pancharatnam-Berry-phase effect. Such distinguished spatial separability of vortex beam carrying different OAM modes can potentially applied to chip-level high-efficiency high-capacity OAM communication, multi-channel optical trapping devices, and 3D parallel laser fabrication.

Acknowledgements

This work is partly supported by the Major Projects of International Cooperation and Exchanges NSFC (No. 61420106014). L.H. and X.S. acknowledge the NSFC Project (No. 61505007) for financial support. L.H. and X.L. acknowledge the NSFC Project (No. 51675049) for financial support. B.R. and T.Z. acknowledges the financial support by the Deutsche Forschungsgemeinschaft (Grant Nos. ZE953/7-1). The authors would like to acknowledge the continuous support from Cedrik Meier by providing the electron beam lithography system.

Received: ((will be filled in by the editorial staff))
Revised: ((will be filled in by the editorial staff))
Published online: ((will be filled in by the editorial staff))

Reference

1. Yu, N. and Capasso, F. Flat optics with designer metasurfaces. Nat. Mater. **13**, 3839 (2014).
2. Meinzer, N., Barnes, W. L. and Hooper, L. R. Plasmonic meta-atoms and metasurfaces. Nat. Photon. **8**, 889-898 (2014).
3. Kildishev, A. V., Boltasseva, A., and Shalaev, V. M. Planar photonics with metasurfaces. Science **339**, 1232009 (2013).
4. Yu, N., Genevet, P., Kats, M. A., Aieta, F., Tetienne, J-P, Capasso, F. and Gaburro, Z. Light propagation with phase discontinuities: generalized laws of reflection and refraction. Science **334**, 333–337 (2012).
5. Ni, X., Emani, N. K., Kildishev, A. V., Boltasseva, A., Shalaev, V. M. Broadband light bending with plasmonic nanoantennas. Science **335**, 427 (2012).
6. Holloway, C. L. et al. An overview of the theory and applications of metasurfaces: The two dimensional equivalents of metamaterials. IEEE Antennas Propagat. Mag. **54**, 10–35 (2012)
7. Pancharatnam, S. Generalized theory of interference and its applications. Proc. Ind. Acad. Sci. A **44**, 247-262 (1956).

8. Berry, M. V. Quantal phase factors accompanying adiabatic changes. Proc. R. Soc. Lond. A **392**, 45-57 (1984).

9. Huang, L., Chen, X., Mühlenbernd, H., Li, G., Bai, B., Tan, Q., Jin, G., Zentgraf, T., and Zhang, S. Dispersionless Phase Discontinuities for Controlling Light Propagation. Nano Lett. **12,** 5750–5755 (2012).

10. Biener, G., Niv, A., Kleiner, V. and Hasman, E. Geometrical phase image encryption obtained with space-variant subwavelength gratings. Opt. Lett. **30**, 1096-1098 (2005).

11. Aieta, F. et al. Aberration-free ultrathin flat lenses and axicons at telecom wavelengths based on plasmonic metasurfaces. Nano Lett. **12,** 4932–4936 (2012).

12. Chen, X., Huang, L., Mühlenbernd, H., Li, G., Bai, B., Tan, Q., Jin, G., Qiu, C-W, Zentgraf, T., and Zhang, S. Dual-polarity plasmonic metalens for visible light. Nat. Comm. **3**,1198 (2012).

13. Khorasaninejad, M., Chen, W.T., Devlin, R. C., Oh, J., Zhu, A. and Capasso, F. Metalenses at visible wavelengths: Diffraction-limited focusing and subwavelength resolution imaging. Science **352**, 1190 (2016).

14. Yu, N., Aieta, F., Genevet, P., Kats, M. A., Gaburro, Z. et al. Broadband, Background-Free Quarter-Wave Plate Based on Plasmonic Metasurfaces. Nano Lett. **12**, 6328-6333 (2012).

15. Pfeiffer, C., Emani, N., Shaltout, M. et al, Efficient Light Bending with Isotropic Metamaterial Huygens' Surfaces. Nano Lett. **14**, 2491 (2014).

16. Huang, L., Chen, X. et al. Three-Dimensional optical holography using a plasmonic metasurface. Nat. Comm. **4**, 2808 (2013).

17. Zheng, G., Mühlenbernd, H., Kenney, M., et al. Metasurface holograms reaching 80% efficiency. Nat. Nanotech. **10**, 308-312 (2015).

18. Jacob, Z., Shalaev, V. M. Plasmonics goes quantum. Science **334**, 463-464 (2011).

19. Krishnamoorthy, H. N. S., Jacob, Z., Narimanov, E., et al. Topological transitions in metamaterials. Science **336**, 205-209 (2012).

20. Yin, X., Ye, Z., Rho, J., Wang, Y. and Zhang, X. Photonic Spin Hall effect at metasurfaces. Science **339**, 1405-1407 (2013).

21. Shitrit, N., Yulevich, I., Maguid, E., Ozeri, D., Veksler, D., Kleiner, V., Hasman, E. Spin-Optical metamaterial route to spin-controlled photonics. Science **340**, 724-726 (2013).

22. Lin, D., Fan, P., Hasman, E., Brongersma, M. Dielectric gradient metasurface optical elements. Science **345**, 298-302 (2014).

23. Arbabi, A., Horie, Y., Bagheri, M. and Faraon, A. Dielectric metasrufaces for complete control of phase and polarization with wubwavlength spatial resolution and high transmission. Nat. Nanotech. **10**, 937-943 (2015).

24. Allen, L., Beijersbergen, M. W., Spreeuw, R. and Woerdman, J. P. Orbital angular momentum of light and the transformation of Laguerre-Gaussian laser modes. Phys. Rev. A **45**, 8185–8189 (1992).

25. Molina-Terriza G., Torres J., and Torner L. Twisted photons. Nat. Phys. **3**, 305–310 (2007).

26. Padgett M. and Bowman R., Tweezers with a twist. Nat. Photon. **5**, 343-348 (2011).

27. Wang, J. et al. Terabit free-space data transmission employing orbital angular momentum multiplexing. Nat. Photon. **6**, 488–496 (2012).

28. Maguid, E., Yulevich, I., Veksler, D., Kleiner, V., Brongersma, M. L. and Hasman, E. Photonic spin-controlled multifunctional shared-aperture antenna array. Science **352**, 1202-1206 (2016).

29. Mehmood ,M., Mei, S., Hussain, S., Huang, K., Siew, S., Zhang, L., Zhang, T., Ling, X., Liu, H., Teng, J., Danner, A., Zhang, S., and Qiu, C. Visible-frequency metasurface for structuring and spatially multiplexing optical vortices. Adv. Mater. **28**, 2533-2539 (2016).

30. Zeng, J., Ling, L., Yang, X. and Gao, J. Generating and separating twisted light by gradient-rotation split-ring antenna metasurfaces. Nano Lett. **16**, 3101-3108 (2016).

31. Ren, H., Li, X., Zhang, Q. and Gu, M. On-chip non-interference angular momentum multiplexing of broadband light. Science **353**, 805-809 (2016).

32. Cai, X., Wang, J., Strain, M. J., Johnson-Morris, B., Zhu, J., Sorel, M., O'Brien, J. L., Thompson, M. G., and Yu, S. Integrated compact optical vortex beam emitters. Science **338,** 363-366 (2012).

33. Bozinovic, N., Yue, Y., Ren, Y., Tur, M., Kristensen, P., Huang, H., Willner, A. E. and Ramachandran, S. Terabit-scale orbital angular momentum mode division multiplexing in fibers. Science **340,** 1545-1548 (2013).

34. Bourennane, M., Karlsson, A. and Björk, G. Quantum key distribution using multilevel encoding. Phys. Rev. A **64**, 012306 (2001).

35. Li, S., and Wang, J. Simultaneous demultiplexing and steering of multiple orbital angular momentum modes. Scientific Reports, **5**, 15406 (2015).

36. Zhang, N., Yuan, X. and Burge, R., Extending the detection range of optical vortices by Dammann vortex gratings. Opt. Lett. **35**, 3495-3497 (2010).

37. Lei, T., Zhang, M., Li, Y. et al. Massive individual orbital angular momentum channels for multiplexing enabled by Dammann gratings. Lig. Sci. & Appl. **4**, e257 (2015).

38. Yu, J., Zhou, C., Jia, W., Hu, A., Cao, W., Wu, J. and Wang S. Generation of dipole vortex array using spiral Dammann zone plates. Applied Optics **51**, 6799-6804 (2012).

39. Li, X., Cao, Y., Tian, N., Fu, L. and Gu, M. Multifocal optical nanoscopy for big data recording at 30 TB capacity and gigabits/second data rate. Optica **2**, 567-570 (2015).

40. Mirhosseini, M., Malik, M., Shi, Z., and Boyd, R. B. Efficient separation of the orbital angular momentum eigenstates of light. Nat. Comm. **4**, 2781 (2013).

41. Genevet, P., Lin, J., Kats, M. A. and Capasso, F. Holographic detection of the orbital angular momentum of light with plasmonic photodiodes. Nat. Comm. **3**, 1278 (2012).

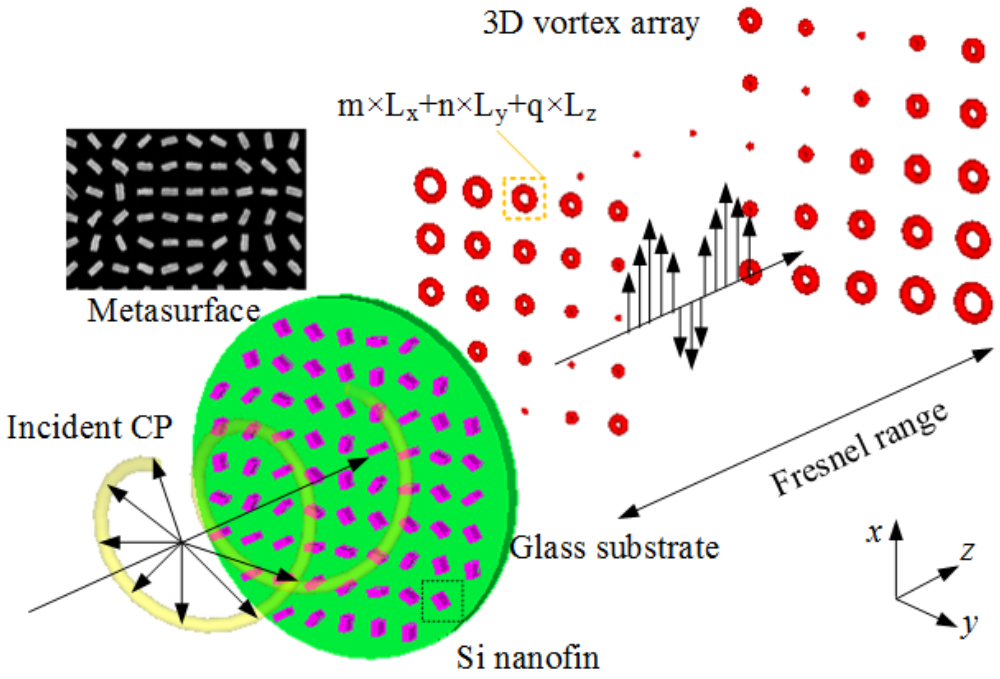

Figure 1. Illustration of the generation and reconstruction procedure of 3D vortex array based on dielectric metasurface. Each Si nanofin plays the role of a pixel of diffractive element, which can generate the required continuous local phase profile with normal incidence of CP light. The reconfigured 3D vortex array with spatially variant topological charges is designed to appear within the Fresnel range.

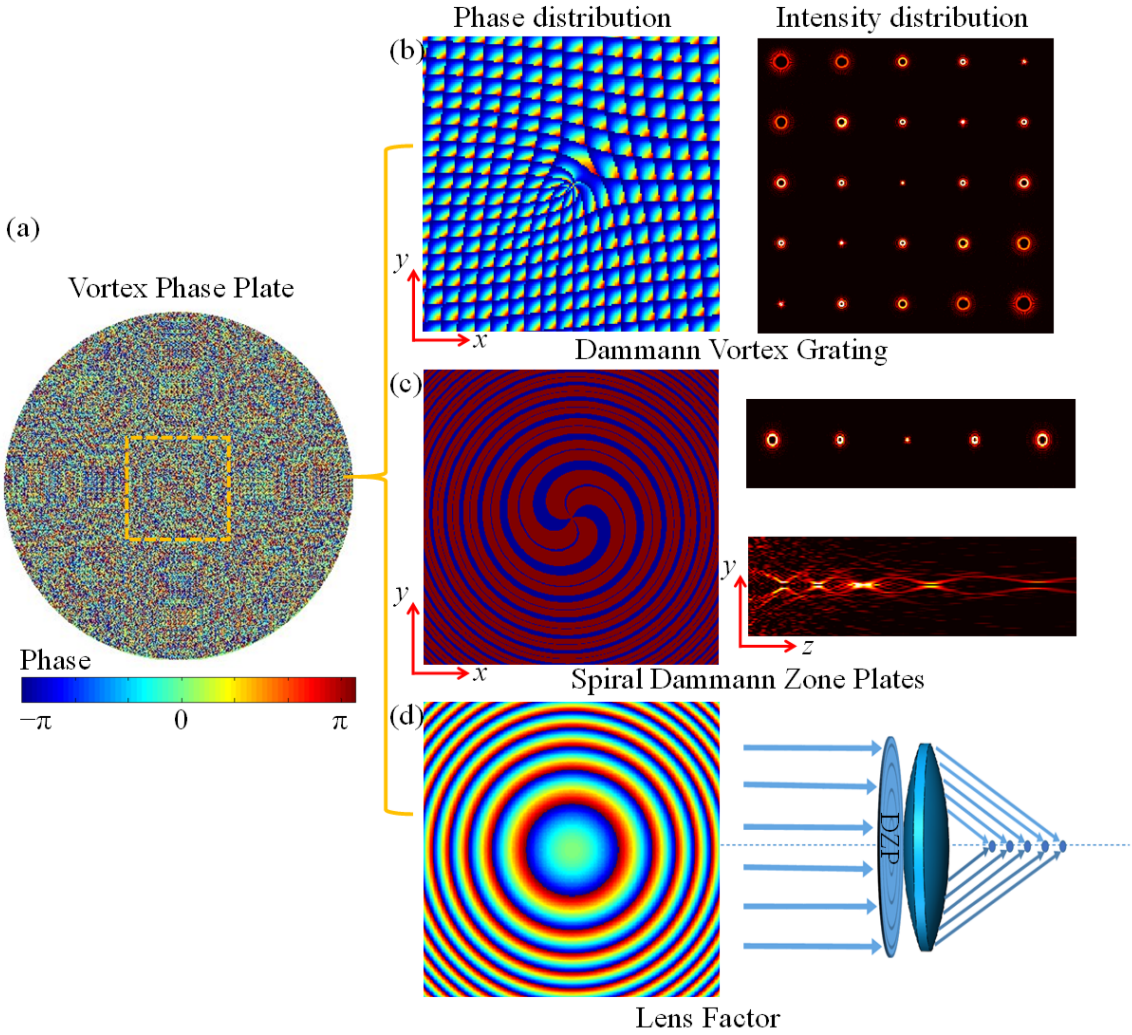

Figure 2. Design principle of the three-dimensional vortex plate. The phase distribution of the 3D vortex plate can be obtained from the combination of an optimized Dammann Vortex Grating, a Spiral Dammann Zone Plate, and a lens factor. For Dammann Vortex Grating, it can generate 2D vortex array in focal plane; and the Spiral Dammann Zone Plate together with a lens factor can generate coaxial space variant vortex array longitudinally along *z* direction.

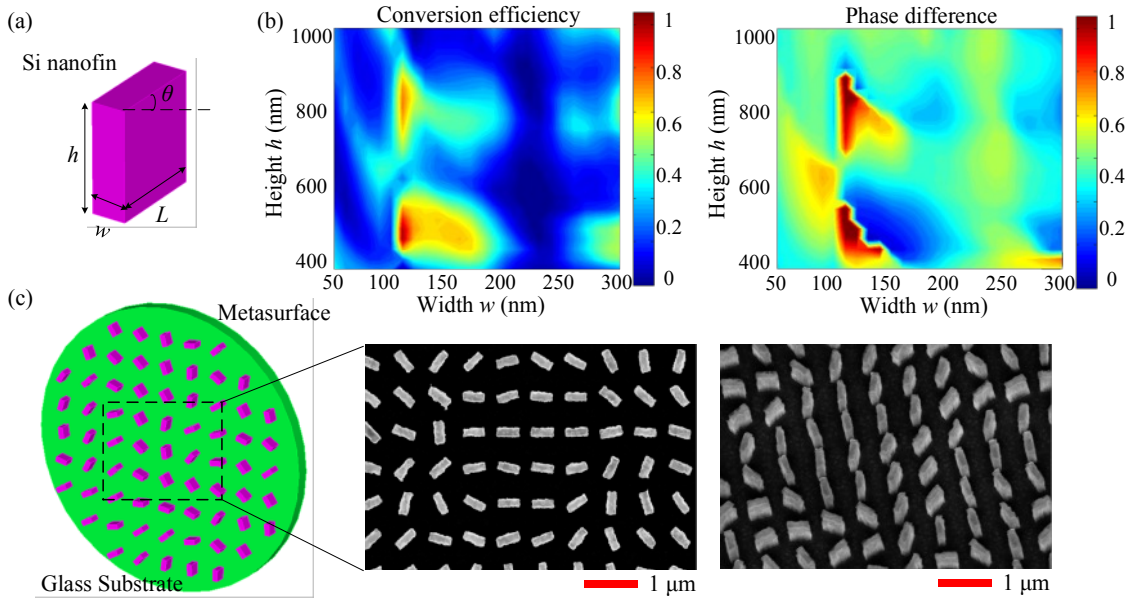

Figure 3. Design of the dielectric metasurface. (a) The schematic structure of dielectric metasurface. It consists of Si nanofin array patterned on glass substrate. The orientation angle φ of the individual nanofin is carrying the desired phase discontinuity. The period of the nanofin array is fixed to be 600 nm, and the length to be 400 nm. The parameters of width and height are swept to achieve half-wave plate at λ=780 nm. (b) Simulated cross polarization conversion efficiency and phase difference δ by sweeping the parameters of width and height of Si nanofin. The operation wavelength is fixed at 780 nm. (c) Schematic of the sample design and scanning electron microscopy images of the fabricated sample (top view and oblique view).

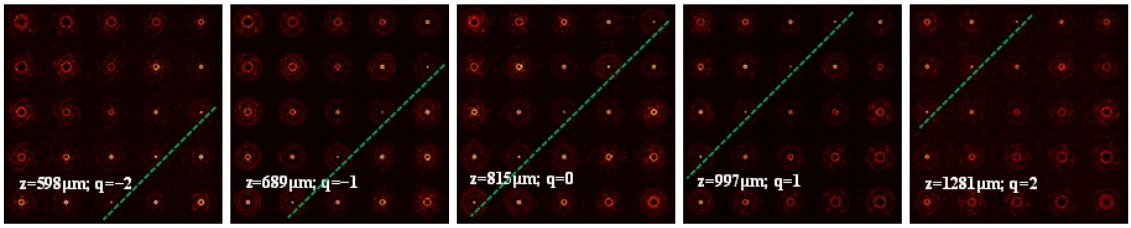

Figure 4. Simulation results of 3D vortex array of each coaxial plane for λ=780 nm. The green dashed lines indicate the positions where the topological charges are equal to zero.

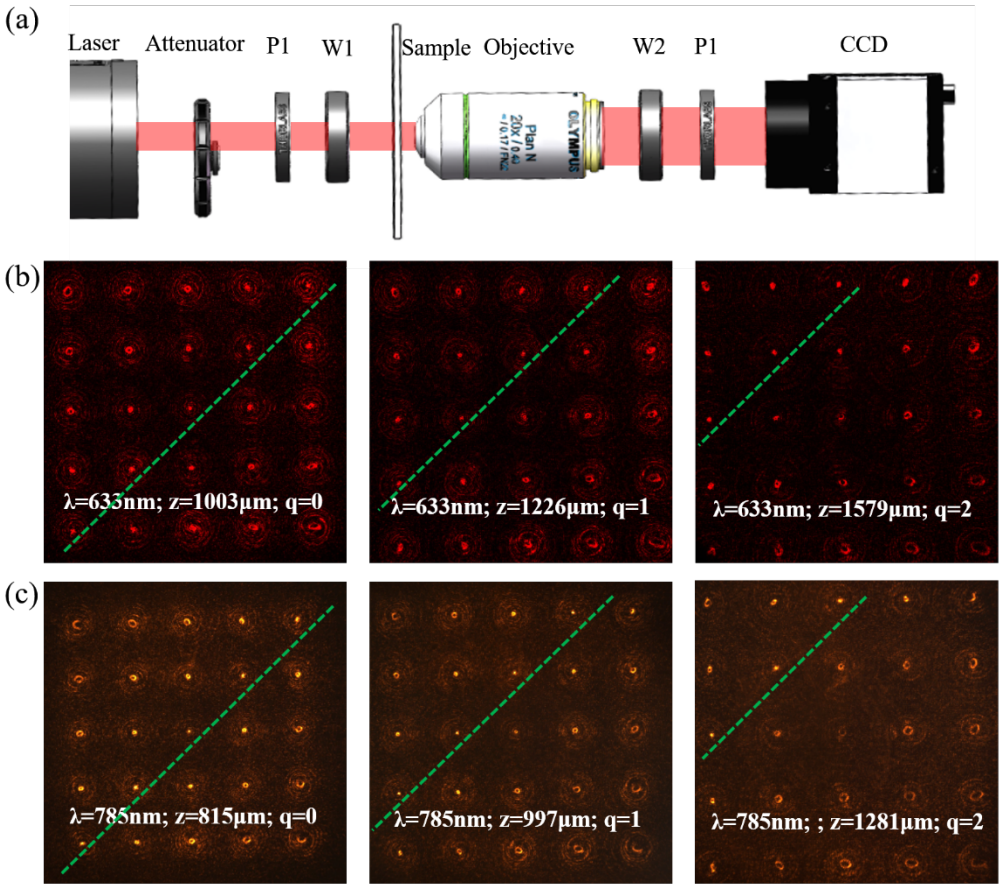

Figure 5. Experimental investigations of 3D vortex array at two different wavelengths. (a) The experiment set up for capturing an image of the 3D vortex array. Different focus planes can be obtained by tuning the distances between the objective and the vortex plate. Experimental results of vortex array at three different *z* positions for *q*=0, 1, 2, respectively, with an incident wavelength of (b) λ=633 nm and (c) λ=780 nm, respectively. The entire set of images can be found in the Supplementary Material. The green dashed lines indicate the location, where the topological charges are equal to zero.

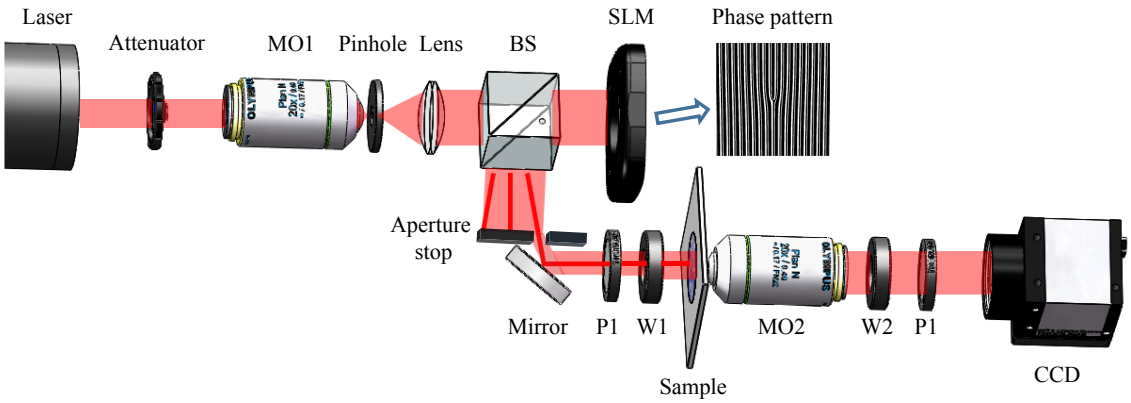

Figure 6. Experimental set up for the detection of topological charges of the vortex array. The spatial light modulator (SLM) uploaded with fork phase profile is used to generate the vortex beam of desired topological charge as incidence beam for the metasurface. After passing through the metasurface sample the 3D vortex array is measured by imaging to a CCD camera (MO-microscopy objective; BS-beam splitter; P-Polarizer; W-quarter wave plate).

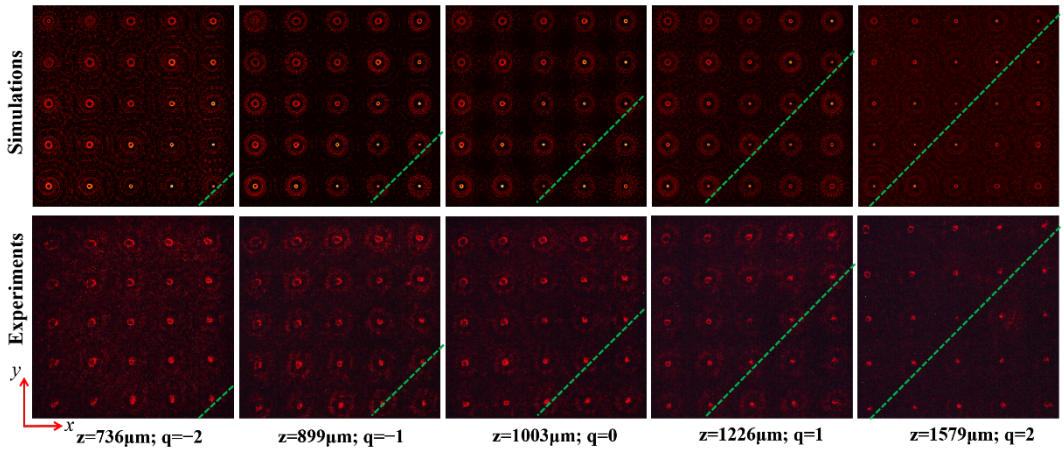

Figure 7. Experimental verification of the space variant topological charges of the 3D vortex array. Simulations results (top row) and experimental results (bottom row) for an incident vortex beam with l=−4 and λ=633 nm for different coaxial observation planes along z direction. The corresponding vortex array with l =4 would be quenched to singularity points for vortices located on the green dashed lines.

Copyright WILEY-VCH Verlag GmbH & Co. KGaA, 69469 Weinheim, Germany, 2013.